ACS OMEGA

http://pubs.acs.org/journal/acsodf

Article

Interactions between Paracetamol and Formaldehyde: Theoretical Investigation and Topological Analysis

Tho Huu Nguyen, Tri Huu Nguyen, Thi Thanh Thuy Le, Hoang Vu Dang,* and Hue Minh Thi Nguyen*

Cite This: *ACS Omega* 2023, 8, 11725−11735

Read Online

ACCESS | Metrics & More | Article Recommendations | Supporting Information

ABSTRACT: In this work, noncovalent interactions including hydrogen bonds, C···C, N···O, and van der Waals forces between paracetamol and formaldehyde were investigated using the second-order perturbation theory MP2 in conjunction with the correlation consistent basis sets (aug-cc-pVDZ and aug-cc-pVTZ). Two molecular conformations of paracetamol were considered. Seven equilibrium geometries of dimers were found from the result of the interactions with formaldehyde for each conformation of paracetamol. Interaction energies of complexes with both ZPE and BSSE corrections range from −7.0 to −21.7 kJ mol^{-1}. Topological parameters (such as electron density, its Laplacian, and local electron energy density at the bond critical points) of the bonds from atoms in molecules theory were analyzed in detail. The natural bond orbital analysis showed that the stability of complexes was controlled by noncovalent interactions including O−H···O, N−H···O, C−H···O, C−H···N, C−H···H−C, C···C, and N···O. The red- and blue-shifted hydrogen bonds could both be observed in these complexes. The properties of these interactions were also further examined in water using a polarized continuum model. In water, the stability of the complex was slightly reduced as compared to that in the gas phase.

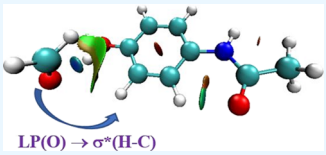

1. INTRODUCTION

Noncovalent interactions such as hydrogen bonds, $\pi-\pi$ stacking, positive charge dipole, etc. play a very crucial role in maintaining the three-dimensional structures of large organic molecules such as proteins and nucleic acids. These interactions also enable one large molecule to bind specifically but transiently to another, making them the basis of many dynamic biological systems.[1−3] In addition, the ability to form hydrogen bonds is one of the essential factors in the bioisosterism process for drug design and optimization.[4] Paracetamol (acetaminophen or *N*-(4-hydroxy phenyl) acetamide, with the chemical formula $C_8H_9NO_2$) is an effective antipyretic and analgesic drug. It is considered as the most prominent analgesic among the acetanilide derivatives. Nowadays, paracetamol has been widely used to replace aspirin due to its excellent pharmacological effects.[5−9]

During the last few decades, the interaction of paracetamol (PAM) with various compounds has attracted the attention of many researchers worldwide. Using the monomer and dimer models of paracetamol with oxalic acid, the generated cocrystal from this mixture was studied by Srivastava et al. by FT-IR and Raman spectroscopies and quantum chemical computations. Accordingly, the structural and spectral calculations indicated that the OH and NH groups of paracetamol formed weaker hydrogen bonds in the cocrystal than those in the pure paracetamol.[10] Misra et al. utilized FT-IR spectroscopy and differential scanning calorimetry to explore the interaction of paracetamol with capric acid and oleic acid. This study evaluated the hydrogen bonding ability between the amino group of paracetamols and the carbonyl group of fatty acids. The polymorphic transition of paracetamol was detected in samples of paracetamol-capric acid but not identified in a mixture of paracetamol with oleic acid.[11] Recently, Zhai et al. have investigated the cooperativity effects of drug−drug intramolecular interactions for the $\pi\cdots\pi$ and H···OH bonds of the phenobarbital···paracetamol···H_2O complex by using density functional theory, MP2 perturbation theory, and statistical thermodynamics. They found that the anti-cooperativity effects of drug−drug intermolecular interactions involving the hydration, $\pi\cdots\pi$ stacking, and H-bonding play an important role in forming the pharmaceutical incompatibility between phenobarbital and paracetamol.[12] In addition, there has been growing interest in hydrogen bonding between paracetamol and other compounds such as water,[13,14] ethanol, acetone,[15] hypromellose,[16] 4,4′−bipyridine,[17] or between paracetamol molecules.[18,19]

The solubility of PAM in CO_2-expanded organic solvents can be explained explicitly through calculations using quantum chemistry. From the local energy-minimum structures of complexes formed by PAM with ethanol or acetone in the 1:1 or 1:3 model and their interaction energies, the interaction of PAM with ethanol was concluded to be slightly stronger as compared to acetone. This finding successfully contributed to

Received: August 15, 2022
Accepted: November 2, 2022
Published: March 22, 2023

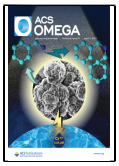

explaining the solubility variation of PAM with CO_2 concentration in acetone and ethanol solvents.[15,20,21]

For multicomponent systems possessing hydrogen bonds such as pharmaceutical cocrystals, vibrational spectroscopy is one of the most useful studying tools.[10,17,22] Recently, molecular structures and hydrogen bond interactions of paracetamol-4,4′-bipyridine cocrystals have been studied by using the vibrational spectroscopic and quantum chemical approach. Srivastava et al. optimized the geometrical structures of complex models constructed from PAM and different organic molecules in many proportions by quantum chemistry calculations. Theoretical analysis of infrared spectra from these optimized geometries successfully assigned vibrational peaks in the infrared data experimentally obtained from cocrystals.[10,17]

In the formulation of pharmaceutical dosage forms, the role of excipients must be comprehensively understood to ensure optimal drug production. Despite being usually thought to be biologically inactive or inert, some excipients may contribute synergistically or antagonistically to pharmaceutically active substance.

Formaldehyde (FMD) is one of the commonly existing impurities in excipients used in pharmaceutical dosage forms such as microcrystalline cellulose, starch, polyethylene glycol, polysorbates, hydroxypropyl cellulose, lactose, and crospovidone. At a trace level of 8 ppm, this compound could generate a 1% hydroxymethyl degradant with the drug substance BMS-203452 in the clinical parenteral formulation (10 mg/mL) upon storage at 5 and 25 °C.[23] This formaldehyde adduct was also found in Avapro film-coated tablets (irbesartan 18.75 and 37.5 mg) during the long-term stability studies, due to the use of propylene glycol in the tablet coating material—Opadry II white.[24] The interaction of the FMD-active principal ingredient was reported for fenfluramine (an anorexic agent that bears a secondary *N*-ethylamine) as evidenced by the conversion into an *N*-methyl derivative.[25] FMD could be formed as the degradation of the drug occurs, altering the bioavailability of pharmaceutical dosage forms, e.g., it was hypothesized by Desai et al. that the hydrolysis of hydrochlorothiazide in the liberation of moisture from excipients produced a small quantity of FMD that reacted with corn starch (to decrease its functionality as a disintegrant) and cross-linked gelatin capsule shells (to form insoluble compounds), leading to poor dissolution and incomplete drug release.[26]

As discussed above, there is a possibility that the interaction between paracetamol and formaldehyde may occur changing the bioavailability properties of paracetamol dosage forms. To the best of our knowledge, little information on such an interaction has been established yet. Therefore, this study aims at investigating the nature of the formed complexes by the interactions of paracetamol with formaldehyde as well as elucidating the electronic properties of these complexes. It is well known that water is a strong polar solvent, common in nature. To approach a situation closer to reality, we therefore investigate the influence of water on the interaction of PAM and FMD using the integral equation formalism polarizable continuum model (IEFPCM). Our research results are expected to better understand the molecular properties of paracetamol pharmaceutical formulations (possibly containing a trace level of formaldehyde) and to assess the impact of hydrogen bonds on the stability of paracetamol−formaldehyde complexes. These parameters would serve as scientific guidance for formulation scientists to predict and select optimal paracetamol dosage forms for better treatment.

2. COMPUTATIONAL METHODS

First, the geometrical structures of formaldehyde, paracetamol monomers, and their dimer complexes were quickly searched by density functional theory with functional B3LYP and the basis set 6-31+G(d). These minima could also be further confirmed using the second-order Moller−Plesset perturbation theory with the calculation level MP2/6-31+G(d). After this, the obtained minima would be further geometrically optimized at the level of MP2 with Dunning's augmented correlation consistent polarized valence double zeta basis set (aug-cc-pVDZ). Many recent studies have shown that MP2 is a good method for studying the properties of compounds containing hydrogen bonds.[27−30] Frequency calculations confirmed that the complexes obtained correspond to true minima. Vibrational frequency, zero-point energy (ZPE), and natural bond orbital (NBO) analysis were calculated at the same level. The hyperconjugative interaction energy $E(2)$ can be calculated from the second-order perturbation theory analysis of the Fock matrix on the NBO basis. For each donor (i) and acceptor (j), the energy $E(2)$ associated with the delocalization $i \rightarrow j$ was determined as follows:

$$E(2) = \Delta E_{ij} = q_i \frac{F_{(i,j)}^2}{\varepsilon_j - \varepsilon_i} \quad (1)$$

where q_i is the donor orbital occupancy, ε_i and ε_j are diagonal elements, and $F(i,j)$ is the off-diagonal NBO Fock matrix element.

For an AB dimer, the interaction energy (ΔE) was defined by the difference between the total energies of the dimer complex and A, B isolated monomers as given in this equation:

$$\Delta E = E_{A\cdots B} - E_A - E_B \quad (2)$$

where $E_{A\cdots B}$, E_A, and E_B mean the total energy of the complex and A, B isolated monomers, respectively. The ZPE corrections are calculated in the present work based on eq 3:

$$\Delta E_{(ZPE)} = E_{A\cdots B(ZPE)} - E_{A(ZPE)} - E_{B(ZPE)} \quad (3)$$

where $E_{A\cdots B(ZPE)}$, $E_{A(ZPE)}$, and $E_{B(ZPE)}$ are the zero-point energies of the complex and A, B monomers, respectively.

The interaction energy was corrected by only ZPE (ΔE) and by both ZPE and basis set superposition error (BSSE) (ΔE^*). The BSSE was corrected by Boys and Bernardi's counterpoise procedure[31] as follows:

$$\Delta E_{(BSSE)} = E_{A\cdots B} - E_A^{A\cdots B} - E_B^{A\cdots B} \quad (4)$$

where $E_{A/B}^{A\cdots B}$ is the calculated energy of the monomer A or B with its geometry in the complex A···B but using the basis functions of the full dimer. The more negative the values of ΔE and ΔE^* are, the more stable the complex is. Furthermore, to more accurately evaluate the energies of the structures, the calculation level with MP2 and aug-cc-pVTZ basis set was used to determine the total energy based on the as-optimized structures. All calculations were performed using the Gaussian 09 suite of programs.[32] Electron density $\rho(r)$ and Laplacian of electron density $\nabla^2\rho(r)$ at bond critical points (BCPs) and ring critical points (RCPs) at MP2/aug-cc-pVDZ geometries were identified using the quantum theory of atoms in the molecule and carried out by the Multiwfn program.[33] The

https://doi.org/10.1021/acsomega.2c05023
ACS Omega 2023, 8, 11725−11735

interaction energy of each hydrogen bond (E_{HB}) was calculated according to the empirical formula of Espinosa−Molins−Lecomte, $E_{HB} = 0.5V(r)$, where $V(r)$ is the localized electron potential density at the BCP.[34] In this study, the IEFPCM model was used to evaluate the influence of solvent on the interaction characteristics of PAM and FMD. Accordingly, the solvent is simulated by a continuous dielectric with the dielectric constant ε, surrounding a cavity whose shape and size are adjusted on the basis of the real geometry of the solute molecule. The solvent creates an electric field that interacts with the solute. The IEFPCM model usually gives good results and has been widely used.[35−38]

3. RESULTS AND DISCUSSION

3.1. Gas Phase. *3.1.1. Structures and Energies.* Paracetamol can exist in many different conformations due to the free rotation of the sigma bond axes. Two molecular conformations of paracetamol, labeled PAM1 and PAM2, were considered in this work. By X-ray diffraction of crystalline paracetamol, it was verified that the PAM2 conformation with the H atoms of the −NH and −OH groups pointing to the same side was the most stable geometry.[39−42] When rotating the C−OH bond axis so that the H atoms of the −NH and −OH groups are in the opposite directions, the PAM1 conformation is formed. The geometries of PAM1 and PAM2 are presented in Figure 1.

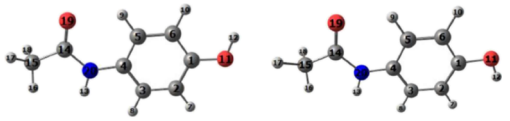

PAM1 PAM2

Figure 1. Two conformations of paracetamol (PAM).

The values of bond lengths and angles of the conformations of PAM at MP2/aug-cc-pVDZ and the measured results from the X-ray experiment are listed in Table 1. As can be seen from Table 1, the results of PAM2 at the MP2/aug-cc-pVDZ level are in reasonable agreement with the experimental values for X-ray diffraction. The mean deviation between our calculation data and experimental results is 0.0726 Å for the bond lengths and 0.4° for the bond angles. The O−H and N−H bond lengths of PAM2 in our calculated results are 0.9679 and 1.0135 Å, respectively. In comparison with other experimental studies, these values are slightly larger than those obtained by Haisa et al. (0.893 and 0.903 Å[39]) but very consistent with those reported by Srivastava et al. (0.9900 and 1.0150 Å[10]). The geometric parameters of PAM1 and PAM2 are similar, except for two bond angles, O11−C1−C2 and O11−C1−C6. The magnitudes of these bond angles are 117.1°, 123.2° for PAM1 and 123.0°, 117.3° for PAM2. The atoms in molecules (AIM) analysis shows that PAM1 and PAM2 both have C5−H9···O19 hydrogen bonds with their electron density $\rho(r)$ and Laplacian $(\nabla^2\rho(r))$ being equal to 0.019 and 0.06 au, respectively. As presented above, in the crystal, paracetamol exists in PAM2; but in terms of energy, at the MP2/aug-cc-pVTZ level, PAM1 has lower energy than PAM2 by ca. 1.2 kJ mol^{-1} after ZPE correction. This value is very small and insignificant. The forming complexes of FMD with PAM were thus studied with both PAM1 and PAM2 conformations.

Seven dimer structures for each conformation of PAM resulted after the consideration of numerous different possibilities of optimization starting points when FMD comes in contact with PAM conformations. Optimized geometrical parameters of the dimers at the MP2/aug-cc-pVDZ are displayed in Figure 2. Each dimer (PAM1, FMD) or (PAM2, FMD) are symbolized hereafter by **A*i*** or **B*i*** ($i = 1 \div 7$), respectively. When the O21 atom of FMD interacts with the H atoms in the same orientation in the O−H and C−H bonds of PAM1 and PAM2, the resulting complexes are

Table 1. MP2/aug-cc-pVDZ Geometries of the Optimized Structures of PAM Conformations in the Gas Phase

	MP2/aug-cc-pVDZ				MP2/aug-cc-pVDZ		
bond length (Å)	PAM)	PAM2	X-ray[42]	bond angle (deg)	PAM1	PAM2	X-ray[42]
C14−O19	1.2352	1.2348	1.232	O19−C14−C15	121.8	121.8	122.5
C14−C15	1.5202	1.5204	1.509	N20−C14−O19	123.8	123.8	122.8
C14−N20	1.3801	1.380	1.340	C4−N20−C14	128.5	128.5	128.3
N20−C4	1.4164	1.4166	1.425	N20−C4−C3	117.1	117.1	116.7
C4−C5	1.4112	1.4131	1.391	C2−C3−C4	121.0	120.8	121.0
C4−C3	1.4136	1.4118	1.389	C1−C2−C3	119.6	119.7	119.9
C3−C2	1.4012	1.4038	1.379	O11−C1−C2	117.1	123.0	122.6
C2−C1	1.4062	1.4069	1.393	O11−C1−C6	123.2	117.3	117.7
C1−O11	1.3819	1.3821	1.377	C5−C6−C1	121.0	120.8	120.1
C1−C6	1.4051	1.4045	1.385	H9−C5−C4	119.9	119.8	118
C6−C5	1.4076	1.4052	1.393	H10−C6−C1	120.0	119.0	120
C5−H9	1.0887	1.0887	0.93	H12−O11−C1	108.5	108.7	107
C6−H10	1.0957	1.0931	0.98	H7−C2−C1	119.4	120.5	120
O11−H12	0.9681	0.9679	0.89	H8−C3−C4	119.7	119.9	118
C2−H7	1.0929	1.0954	0.95	H13−N20−C14	116.2	116.1	114
C3−H8	1.0958	1.0958	0.96	H17−C15−C14	108.3	108.3	110
N20−H13	1.0136	1.0135	0.90	H16−C15−C14	113.5	113.6	112
C15−H17	1.0990	1.0993	0.93				
C15−H16	1.1000	1.1000	0.88	H18−C15−C14	108.4	108.4	109
C15−H18	1.1007	1.1000	1.07				
O19···H9	2.1988	2.2015	2.38				

https://doi.org/10.1021/acsomega.2c05023
ACS Omega 2023, 8, 11725−11735

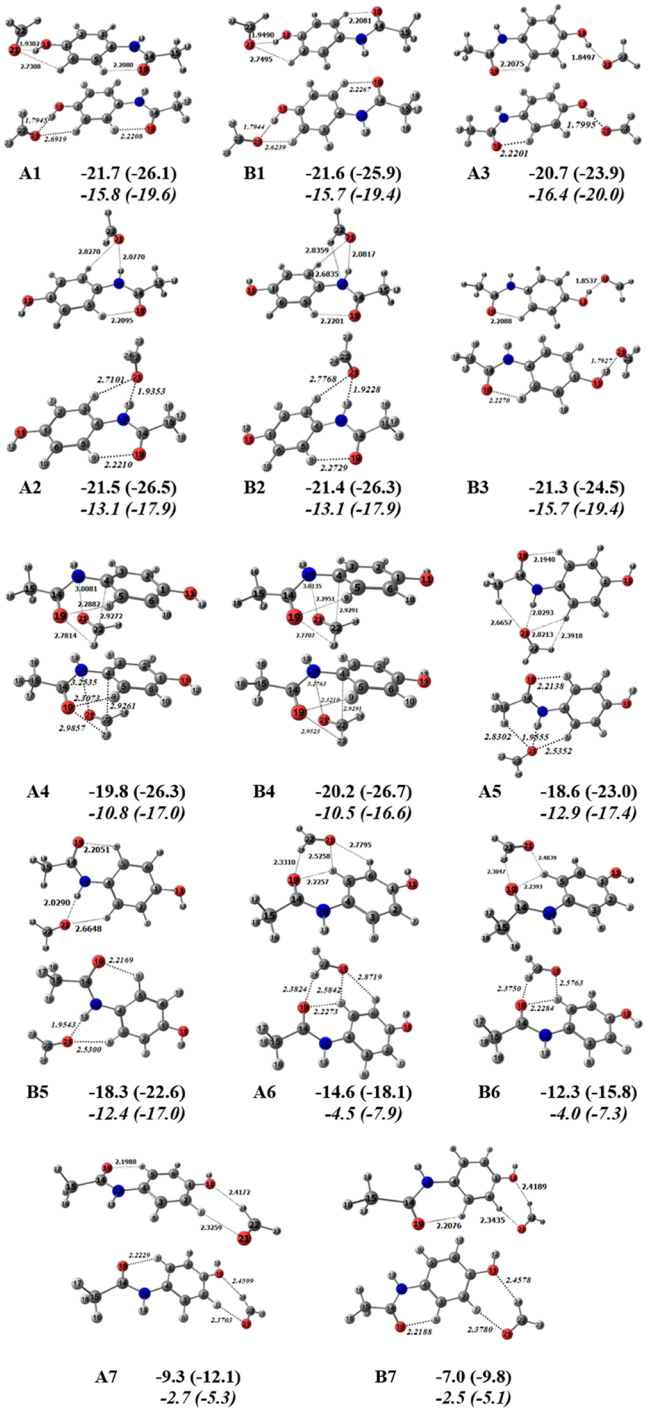

Figure 2. Geometries of the optimized structures of the complexes pairing PAM with FMD at MP2/aug-cc-pVDZ. For each structure, the geometry is displayed above for the gas phase and below for the water solvent with the values for bond length (Å) and interaction energy ΔE^* (kJ mol^{-1}); the values given in brackets are ΔE, and the values in italics are for the water solvent.

denoted **A1** and **B1**, respectively. When the interaction involving the H atoms of N−H and C−H aromatic rings with the molecular planes of PAM and FMD at the positions that tend to be perpendicular to each other, we get complexes **A2** and **B2**. If O21 only interacts with H in O−H, we get **A3** and **B3**. The structure of PAM contains a π-system phenol and a highly polar acetamide −NH−(CH$_3$)C═O group, which is favorable for the formation of noncovalent interactions through the charge transfer of π-orbitals with FMD as two molecules stack to each other, the resulting complexes are called **A4** and **B4**. It was noteworthy that in the process of determining the minima of the dimer complex, the structures **A4** and **B4** could not be determined by density functional theory at the level of B3LYP/6-31+G(d), even only with the higher basis set of B3LYP/aug-cc-pVDZ. They could only be found by second-order Moller−Plesset perturbation theory or density functional theory with functional M06-2X. The geometry of **A4** and **B4** at the M06-2X/aug-cc-pVDZ level is also shown in Figure S3 of the Supporting Information (SI) file. Provided that PAM and FMD still tend to belong to the same plane, we will get **A5** and **B5** complexes when the contact involves the H atom of the N−H with the C−H bond of aromatic rings but **A7** and **B7** when the contact involves both O and H atoms in FMD. On the other hand, we have **A6** and **B6** complexes when the O atom of the carbonyl functional group in PAM participates in the contact.

As displayed in Figure 2, the contact distances of H···O in O−H···O, N−H···O, and C−H···O interactions of all the complexes, except **A4** and **B4**, are in the range of 1.8497−1.9490, 2.0293−2.0817, and 2.1940−2.8359 Å, respectively. These values are smaller than the sum of the van der Waals radius of H and O atoms, 2.72 Å,[43] suggesting that there is the formation of hydrogen bonds in the complexes mentioned. In contrast, the distances of H···O of C−H···O interactions in **A1**, **A2**, **B1**, **B2**, **A4**, **B4**, **A5**, and **A6** (in the range of 2.7308−2.8359 Å) are slightly larger than the sum of the van der Waals radius even though hydrogen bonds can still exist in these interactions. The explanation is that these hydrogen bonds share the proton acceptor O21 atom with the neighboring hydrogen bonds, which may cause the anti-cooperativity effect to prolong the interaction distances.[44] For **A4** and **B4** complexes, the O21···N20 and C4−C22 contact distances are of 3.0081, 2.9272, and 3.0135, 2.9291 Å, respectively; they are also smaller than the sum van der Waals radius of the two atoms participating in the interactions (3.07 and 3.40 Å for the corresponding pairs of N and O, C and C atoms[43]). As a consequence, the noncovalent interactions in these complexes were generated. Concomitant with this formation, the XHY angles are in the range of 102.1−179.7° (greater than 90° as displayed in Table S1 of the SI file), which is the limiting threshold for hydrogen bond generation. In brief, the above observations lead to a rough prediction that the hydrogen bond formation from PAM and FMD occurred.

The interaction energies of all the complexes are also shown in Figure 2. These interaction energy values are quite negative, from −9.8 to −26.1 kJ mol^{-1} with ZPE correction and from −7.0 to −21.7 kJ mol^{-1} with both ZPE and BSSE corrections, showing that the complexes are quite stable. The most stable complexes are **A1** and **B1** because they have the lowest interaction energies. The ΔE^* values are of −21.7 and −21.6 kJ mol^{-1} for **A1** and **B1**, respectively. Excluding the BSSE correction, the ΔE values are of −26.1 and −25.9 kJ mol^{-1} for **A1** and **B1**, respectively, very close to the interaction energies of PAM with water when calculated at the MP2/6-311++G(d,p) level, −26.3 kJ mol^{-1}[13] This suggests that the interaction ability of paracetamol with either water or formaldehyde is the same.

The interaction energies of **A1**, **B1**, **A2**, **B2**, and **B3** complexes are very close to each other (only 0.1 kJ mol^{-1} apart) so that they have almost the same stability, indicating their possible coexistence. The next group including **A3**, **B4**,

https://doi.org/10.1021/acsomega.2c05023
ACS Omega 2023, 8, 11725−11735

Table 2. Electron Density ($\rho(r)$), Laplacian ($\nabla^2\rho(r)$), Local Electron Energy Density $H(r)$, and Hydrogen Bond Energy (E_{HB}) at BCPs of PAM and Complexes at MP2/aug-cc-pVDZ in the Gas Phase

system	interaction	$\rho(r)$ (au)	$\nabla^2\rho(r)$ (au)	$H(r)$ 10^{-3} (au)	E_{hB} (kJ mol^{-1})
PAM1	C5−H9···O19	0.019	0.06	0.058	−20.3
PAM2	C5−H9···O19	0.019	0.06	0.062	−20.2
A1	O11−H12···O21	0.027	0.09	0.478	−27.7
	C6−H10···O21	0.007	0.03	0.899	−6.0
	C5−H9···O19	0.019	0.06	0.078	−20.0
A2	N20−H13···O21	0.022	0.06	−0.469	−21.8
	C3−H8···O21	0.006	0.02	0.861	−4.8
	C5−H9···O19	0.019	0.06	0.064	−19.9
A3	O11−H12···O21	0.029	0.12	3.571	−30.1
	C5−H9···O19	0.018	0.07	0.657	−19.6
A4	C···C[a]	0.011	0.04	1.764	
	O···N	0.010	0.03	0.494	
	C22−H23···O19	0.007	0.03	1.262	−5.2
	C5−H9···O19	0.017	0.06	0.536	−17.9
A5	N20−H13···O21	0.019	0.07	2.195	−18.4
	C15−H16···O21	0.005	0.02	0.991	−5.1
	C3−H8···O21	0.005	0.02	0.899	−4.4
	C22−H24···H8−C3	0.004	0.02	1.020	−3.4
	C5−H9···O19	0.019	0.07	0.658	−20.2
A6	C22−H24···O19	0.010	0.04	0.719	−10.5
	C6−H10···O21	0.005	0.02	1.014	−4.4
	C5−H9···O21	0.009	0.03	0.737	−8.8
	C5−H9···O19	0.018	0.06	0.613	−19.5
A7	C22−H24···O11	0.010	0.03	0.383	−9.5
	C2−H7···O21	0.013	0.04	−0.127	−12.4
	C5−H9···O19	0.019	0.06	0.063	−20.3
B1	O11−H12···O21	0.027	0.08	0.231	−27.1
	C2−H7···O21	0.007	0.03	0.975	−5.8
	C5−H9···O19	0.019	0.06	0.074	−20.0
B2	N20−H13···O21	0.021	0.06	−0.490	−21.6
	C3−H8···O21	0.006	0.02	0.878	−4.7
	C22−H24···N20	0.008	0.03	1.246	−7.7
	C5−H9···O19	0.019	0.06	0.094	−19.5
B3	O11−H12···O21	0.031	0.11	1.426	−31.8
	C5−H9···O19	0.019	0.06	0.065	−19.9
B4	C···C	0.011	0.04	1.762	
	O···N	0.010	0.03	0.501	
	C22−H23···O19	0.007	0.03	1.265	−5.3
	C5−H9···O19	0.017	0.06	0.562	−17.6
B5	N20−H13···O21	0.020	0.07	1.058	−19.8
	C3−H8···O21	0.006	0.02	0.861	−5.2
	C5−H9···O19	0.019	0.06	0.049	−20.1
B6	C5−H9···O21	0.010	0.03	0.367	−9.7
	C22−H24···O19	0.012	0.04	0.432	−11.9
	C5−H9···O19	0.018	0.06	0.087	−19.2
B7	C22-H24···O11	0.010	0.03	0.395	−9.5
	C6−H10···O21	0.013	0.04	−0.083	−11.8
	C5−H9···O19	0.019	0.06	0.078	−19.9

[a]C···C represents O21−C22···C4−C5 in **A4** and O21−C22···C4−C3 interaction in **B4**, and O···N represents C22−O21···N20 in **A4**, **B4**.

A4, **A5**, and **B5** has ΔE^* in the range from −20.7 to −18.3 kJ mol^{-1}. If only ZPE is corrected, the lowest interaction energies are obtained for **A4** and **B4** complexes, i.e., −26.3 and −26.7 kJ mol^{-1}, respectively. The largest interaction energies are observed for the remaining complexes, **A6**, **B6**, **A7**, and **B7**, in the range from −14.6 to 7.0 kJ mol^{-1}. As shown in Figure 2, the complexes have a decreasing order of strength as follows: **A1** > **B1** > **A2** > **B2** > **B3** > **A3** > **B4** > **A4** > **A5** > **B5** > **A6** > **B6** > **A7** > **B7**. For the first 10 dimers of this order, the deviation in interaction energies is negligible between **A1** and **B5** complexes, only ca. 3.4 kJ mol^{-1}. In general, the stability of complexes does not depend much on the conformation of paracetamol.

3.1.2. Topological Analysis. The "atoms in molecules" topological analysis (AIM) of the electron density helps validate the existence of noncovalent interaction in all the structures. This work provides basic understanding on the interactions of complexes. For hydrogen bond formation, three

https://doi.org/10.1021/acsomega.2c05023
ACS Omega 2023, 8, 11725−11735

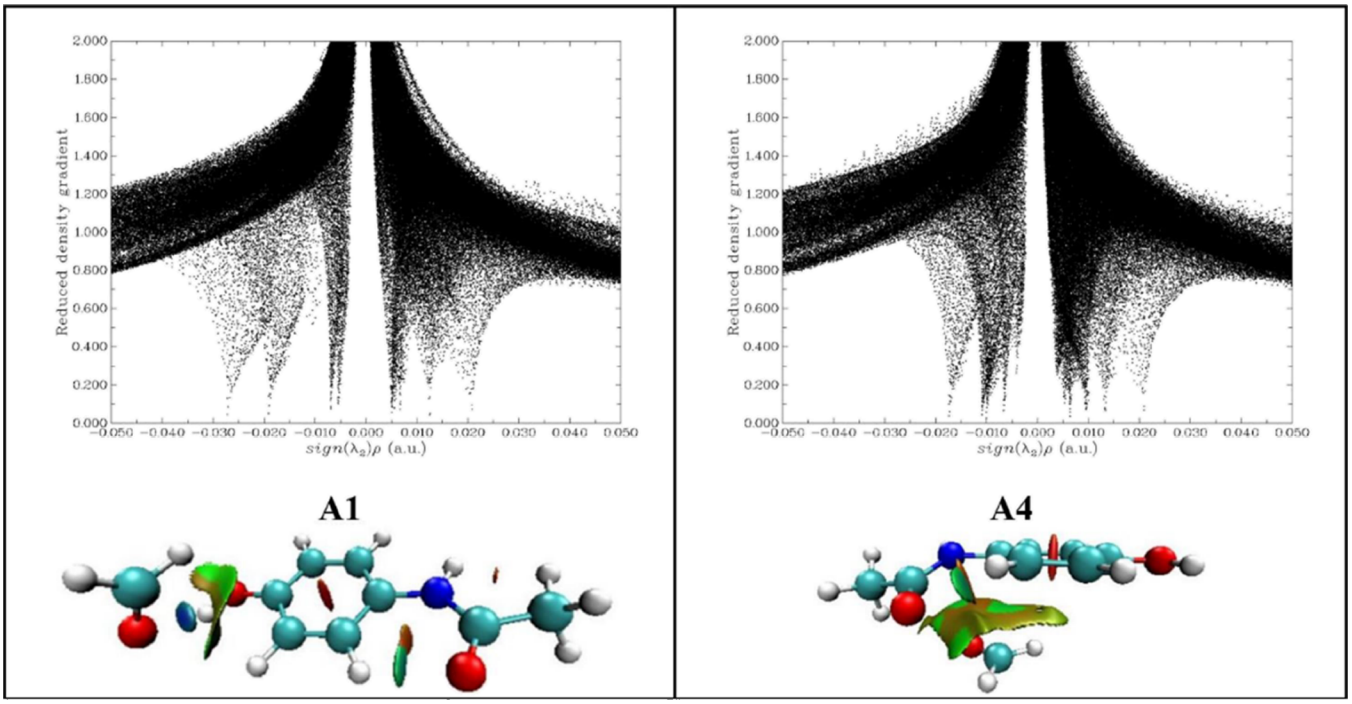

Figure 3. RDG versus sign(λ_2)ρ plots for **A1** and **A4** complexes in the gas phase. 2D/on 3D/under, the surfaces are colored on a blue-green-red scale according to the values of sign(λ_2)ρ, (s = 0.5 au).

different criteria out of eight as proposed by Popelier[45] are most often applied, i.e., (i) a BCP to classify an interaction as a hydrogen bond; (ii) the electron density $\rho(r)$ at the BCP in the range of 0.002−0.040 au, and (iii) the Laplacian $\nabla^2\rho(r)$ at the BCP in the range of 0.02−0.15 au. The value of $\rho(r)$ is used to measure the strength of a bond. Linear relationships are found between the magnitude of $\rho(r)$ and the length of a hydrogen bond. In general, the larger the magnitude of $\rho(r)$ is, the stronger the bond is.[46,47] If bonds have large values of $\rho(r)$ and $\nabla^2\rho(r) < 0$, they are polar and nonpolar covalent interactions; in contrast, small values $\rho(r)$ and $\nabla^2\rho(r) > 0$ correspond to closed-shell interactions.

The AIM molecular graph in Figure S1 shows the presence of BCPs or RCPs at the junction of PAM and FMD. All of the optimized complex structures have BCPs for X−H···Y (X = O, N, and H; Y = O, N, and H−C) intermolecular hydrogen bond formation. Although the H24···H8 contact distance of **A5** is quite large (2.3918 Å), it is still slightly smaller than the sum of the van der Waals radius of the two hydrogen atoms. The critical point is also detected for this distance, which is a dihydrogen bond, C−H···H−C form. Similarly, the H···N contact distance in the C−H···N interaction of **B2** is 2.8359 Å, which is slightly larger than the sum of the van der Waals radius of the two N and H atoms, 2.72 Å, but still existing at a critical point for this distance.

Most remarkably, we find more BCPs of the C···C intermolecular contact (O21−C22···C4−C5 interaction in **A4** and O21−C22···C4−C3 interaction in **B4**) and O···N contact in both **A4** and **B4** structures. The topological parameters for the complexes are given in Table 2. The $\rho(r)$ and $\nabla^2\rho(r)$ values in BCP of X−H···Y are in the range of 0.004−0.031 and 0.02−0.12 au, respectively. Both values fall within the criterion range of hydrogen bond formation. These values of the C5−H9···O19 intramolecular hydrogen bonds of all the complexes are not much different, changing very little from that of the monomer, in the range 0.017−0.019 and 0.06−0.07 au. Table 2 shows that the $\rho(r)$ values at BCPs for O−H···O (0.027−0.031 au) and N−H···O (0.019−0.022 au) are larger than those for C···C (0.010−0.011 au), O···N (0.010 au) and much larger than those at BCPs for C−H···N (0.008 au), C−H···O (intermolecular, 0.005−0.013 au), or C−H···H−C (0.004 au). Although the electron density and Laplacian at the critical points C2−H7···O21 of **B1**, C3−H8···O21 of **A2**, **B2**, **A5**, and **B5**, C6−H10···O21 of **A1** and **A6**, and C22−H23···O19 of **A4** and **B4** lie within the recommended range for hydrogen bonding, these values are all very small, 0.005−0.007 and 0.02−0.03 au, respectively. This is consistent with quite a long distance between the atoms participating in the bond, 2.7308−2.8359 Å. Therefore, the strength and contribution to the complex strengthening of the bonds can be arranged in the following order: O−H···O > N−H···O > C···C, O···N, C−H···O/N/(H−C).

In the case of complexes, the interaction energies E_{HB} of the O−H···O hydrogen bond (from −27.1 to −31.8 kJ mol^{-1}) are more negative than those of N−H···O bonds (from −21.8 to −18.4 kJ mol^{-1}) and much more negative than those of the C−H···O intermolecular hydrogen bond (ca. from −4.4 to −12.4 kJ mol^{-1}), C−H···N bonds (−7.7 kJ mol^{-1}), and C−H···H−C bonds (−3.4 kJ mol^{-1}). This again demonstrates that the stability of the bonds decreases in the direction of O−H···O > N−H···O > C−H···O/N/(H−C). Notably, the E_{HB} energy of the C5−H9···O19 intramolecular hydrogen bond (−17.6 to −20.3 kJ mol^{-1}) is also much more negative than those of the C−H···O intermolecular hydrogen bond (−4.4 to −12.4 kJ mol^{-1}). Thus, with reference to hydrogen bonding C−H···O, the intramolecular interaction is demonstrated to be more stable than the intermolecular interaction in the investigated complexes.

In order to visualize a possible formation of weak interactions between PAM and FMD, the noncovalent

https://doi.org/10.1021/acsomega.2c05023
ACS Omega 2023, 8, 11725−11735

Table 3. EDT and Hyperconjugative Interaction Energy $E(2)$ (kJ mol^{-1}) for Complexes at MP2/aug-cc-pVDZ in the Gas Phase

complex	interaction	EDT (e)	$E(2)$	complex	interaction	EDT (e)	$E(2)$
A1	O11−H12···O21	0.0177	50.6	**B1**	O11−H12···O21	0.0163	46.4
	C6−H10···O21		0.6		C2−H7···O21		0.7
	C5−H9···O19		11.7		C5−H9···O19		11.8
A2	N20−H13···O21	0.0164	38.0	**B2**	N20−H13···O21	0.0160	37.2
	C3-H8···O21		0.3		C3−H8···O21		0.3
	C5−H9···O19		11.8		C22−H24···N20		0.8
					C5−H9···O19		11.0
A3	O11−H12···O21	0.0235	69.7	**B3**	O11−H12···O21	0.0231	68.5
	C5−H9···O19		12.0		C5−H9···O19		11.9
A4	O21−C22···C4-C5	−0.0085	11.7	**B4**	O21−C22···C4-C3	−0.0083	11.5
	C22−O21···N20		0.5		C22−O21···N20		0.5
	C22−H23···O19		0.4		C22−H23···O19		0.4
	C5−H9···O19		5.7		C5−H9···O19		5.5
A5	N20−H13···O21	0.0188	46.1	**B5**	N20−H13···O21	0.0184	45.6
	C15−H16···O21		2.5				
	C3−H8···O21		0.8		C3−H8···O21		3.1
	C22−H24···H8-C3		1.5		C5−H9···O19		12.2
	C5−H9···O19		12.8				
A6	C22−H24···O19	0.0048	11.5	**B6**	C5−H9···O21	0.0048	4.9
	C6−H10···O21		1.7		C22−H24···O19		11.8
	C5−H9···O21		3.1		C5−H9···O19		10.8
	C5−H9···O19		11.4				
A7	C22−H24···O11	0.0066	9.2	**B7**	C22−H24···O11	0.0063	9.0
	C2−H7···O21		16.5		C6−H10···O21		15.7
	C5−H9···O19		12.3		C5−H9···O19		11.9

interactions (NCI) technique was also implemented. The NCI index points out interactions in a structure based solely on the electron density and its derivatives. When a weak inter- or intramolecular interaction is present, there is a crucial change in the reduced gradient between interacting atoms, producing density critical points between interacting fragments. The dependence of reduced density gradient (RDG) $s(r)$ on the electron density $\rho(r)$ follows the following equation.[48,49]

$$s(r) = \frac{1}{2(3\pi^2)^{1/3}} \frac{|\nabla\rho(r)|}{\rho(r)^{4/3}} \quad (5)$$

where $\nabla\rho(r)$ is the first derivative of $\rho(r)$.

The Laplacian of the electron density, $\nabla^2\rho(r)$, is often decomposed into a sum of contributions along the three principal axes of maximal variation, i.e., the three eigenvalues λ_1, λ_2, and λ_3 of the electron density Hessian matrix. The sign of λ_2 can be used to distinguish bonded ($\lambda_2 < 0$) from nonbonded ($\lambda_2 > 0$) interactions.[48] The strength of a weak interaction is known to be proportional to the electron density in the corresponding region. The van der Waals interaction regions always have a very small electron density, while the regions corresponding to a strong steric effect and hydrogen bonding always possess a larger electron density. The NCI technique uses two quantities including sign$(\lambda_2)\rho(r)$, that is the sign of λ_2 multiplied by $\rho(r)$, and RDG $s(r)$ to map these interaction properties.

The 2D and 3D NCI plots of **A1** and **A4** representative complexes are depicted in Figure 3 (the others are displayed in Figure S2 of the SI file). For the 2D plots, on the X-axis, peaks with a negative sign $(\lambda_2)\rho(r)$ correspond to noncovalent interactions whereas peaks with positive large values correspond to steric repulsions. The 2D plot of **A1** has three sharp peaks at the value of sign$(\lambda_2)\rho(r)$, i.e., −0.00272, −0.0191, and −0.0070 au, respectively, corresponding to the interactions O11−H12···O21, C5−H9···O19, and C6−H10···O21. On the right-hand side of the peak of C6−H10···O21 is a peak with sign$(\lambda_2)\rho(r)$ slightly larger than −0.0070 au, being ascribed to interaction linked van der Waals forces. A similar behavior can be observed in **A4**, i.e., there are four peaks of interactions C5−H9···O19, C22···C4, O21···N20, and C22−H23···O19 between −0.0066 and −0.0174 au of sign$(\lambda_2)\rho(r)$.

The 3D plots in Figures 3 and S2 are created using Visual Molecular Dynamics,[50] with gradient isosurfaces s = 0.5 au, and the geometric orientation and atomic numbering of the complexes are similar to those shown in Figure 2. The red zones of the RGD isosurface correspond to repulsive interactions and these regions have positive sign$(\lambda_2)\rho(r)$. In these complexes, they are located in the center of the benzene ring and the center of the ring formed from H9, C5, C4, N20, C14, and O19 atoms or from H13, H16, C15, C14, and N20 atoms (except **A4** and **B4**). The regions having negative λ_2 values are blue zones, where attractive noncovalent interactions (such as hydrogen bonds) exist. Accordingly, the more blue shift means the stronger interactive interaction. The green surfaces are zones where the value of λ_2 is close to zero and represent the regions of weak, delocalized interactions. The zones of O−H···O are in a darker shade of blue than those of N−H···O interactions while of C···C, O···N, and C−H···O/N/(H−C) interactions are all green. It can be seen that in **A1**, there are also green zones between H24 and C1−C6 or between H13 and H16 atoms. Similarly in **A4**, in addition to the green zones corresponding to the interactions C22···C4, O21···N20, C22−H23···O19, and C5−H9···O19, there are also green zones between O21 and H17 as well as H24 and the benzene ring, representing the van der Waals forces. The electron density at these interatomic contacts is so small that

https://doi.org/10.1021/acsomega.2c05023
ACS Omega 2023, 8, 11725−11735

BCPs do not appear at these interactions in the AIM analysis. They can only be observed using the NCI technique.

3.1.3. NBO Analysis. NBO analysis provides an efficient tool for studying intra- and intermolecular bonding and interaction among bonds. It also gives a distinct basis for investigating charge transfer or conjugative interaction in molecular systems. In this study, the NBO analysis is performed at the MP2/aug-cc-pVDZ level, the results are shown in Table 3. In the complexes with lower interaction energies ΔE^*, including **A1**, **B1**, **A2**, **B2**, **A3**, **B3**, and **A5**, **B5**, their electron density transfer (EDT) are all positive, in the range of 0.0160−0.0235e, larger than those of **A6**, **B6**, **A7**, and **B7**. The EDT occurs mainly from the lone pairs on the O21 atom of FMD to the antibonding orbital σ^*(O/N−H) of PAM. Their $E(2)$ values are quite large, i.e., about 46.4−69.7 kJ mol^{-1} for O11−H12···O21 but slightly smaller for N20−H13···O21 ca. 37.2−46.1 kJ mol^{-1}. Meanwhile, for the complexes **A6**, **B6**, **A7**, and **B7**, the stability is determined only by the C−H···O hydrogen bonds. The $E(2)$ value of C2−H7···O21 in **A7** is only 16.5 kJ mol^{-1}, this is also the C−H···O hydrogen bond with the largest $E(2)$ value of all the complex structures found in this study. They are also consistent with the AIM analyses above, and $\rho(r)$ and Laplacian $\nabla^2\rho(r)$ of these hydrogen bonds are also smaller and their E_{HB} are also much more positive than those of the O/N−H···O hydrogen bonds of **A1**, **B1**, **A2**, **B2**, **A3**, **B3**, and **A5**, **B5**.

In particular, the data in Table 4 show that the stability of **A4** and **B4** complexes is generated from the exchange of electrons between PAM and FMD. Their negative EDT values indicate that the electron density transfer from PAM to FMD is more dominant, in contrast to all other complexes.

Table 4. Some Hyperconjugative Interaction Energies in A4 and B4 Complexes in the Gas Phase

complex	donor NBO (i)	acceptor NBO (j)	$E(2)$ kJ mol^{-1}
A4	π(C4−C5)	π^*(O21−C22)	11.7
	π^*(C4−C5)	π^*(O21−C22)	1.5
	π(C14−O19)	π^*(O21−C22)	1.1
	π(C14−O19)	σ^*(C22−H23)	0.4
	LP(N20)	π^*(O21−C22)	0.5
	π(O21−C22)	π^*(C4−C5)	2.3
	π(O21−C22)	π^*(C14−O19)	3.0
	LP(O21)	π^*(C14−O19)	2.6
B4	π(C3−C4)	π^*(O21−C22)	6.2
	π^*(C3−C4)	π^*(O21−C22)	5.4
	π(C5−C6)	σ^*(O21−C22)	1.0
	π(C5−C6)	π^*(O21−C22)	1.1
	π(C14−O19)	π^*(O21−C22)	1.1
	LP(N20)	π^*(O21−C22)	0.5
	π^*C5−C6)	π^*(O21−C22)	2.6
	π(C14−O19)	σ^*(C22−H23)	0.4
	π(O21−C22)	π^*(C3−C4)	2.0
	π(O21−C22)	π^*(C14−O19)	2.9
	LP(O21)	π^*(C14−O19)	2.6

Furthermore, for **A4**, the electron transfer mainly occurs from π(C4−C5) → π^*(O21−C22). The $E(2)$ value of this process is 11.7 kJ mol^{-1}. The reverse transfer π(O21−C22) → π^*(C4−C5) has a much smaller $E(2)$ energy, 2.3 kJ mol^{-1}. These two transfers contribute mainly to the C···C interaction of **A4**. Although the $\rho(r)$ and Laplacian $\nabla^2\rho(r)$ values at the BCP of O···N in C22−O21···N20 interaction are not much different from those of C···C in O21−C22···C4−C5 interaction, the $E(2)$ of the process LP(N20) → π^*(O21−C22) is very small, only about 0.5 kJ mol^{-1}. This is because the nonbonding orbital of the N20 atom with the π orbitals of the C4−C5 and C14−O19 bonds are in sites where the conjugation effect can be formed; the delocalized electrons of the π(C4−C5) and π(C14−C19) orbitals also supplement the electron transfer LP(N20) → π^*(O21−C22), thereby increasing the value of $E(2)$. For the C22−H23···O19 hydrogen bond of A4, its $E(2)$ value is very small, 0.4 kJ mol^{-1}, only larger than that of the C3−H8···O21 hydrogen bond of **A2** and **B2**. It is consistent with its electron density $\rho(r)$ at the BCP, also very small, 0.007 au (as analyzed above by AIM). For all the hydrogen bonds above, the bonding is formed by EDT due to the process LP(Y) → σ^*(X−H), but in this hydrogen bond we detect that a direct electron transfer into σ^*(C22−H23) comes mainly from π(C14−O19), which is affected by the conjugation effect with a nonbonding orbital of N20 and π(C4−C5) orbitals.

The formation of O21−C22···C3−C4, C22−O21···N20, and C22−H23···O19 interactions in **B4** could be explained in a similar manner to that of **A4**. This **B4** complex is stabilized by π(C3−C4) → π^*(O21−C22), π^*(C3−C4) → π^*(O21−C22) transfers, plus LP(N20) → π^*(O21−C22), π(C14−O19) → σ^*(C22−H23) transfers.

By comparing the hyperconjugative interaction energy $E(2)$ of the above bonds, we also get the same results as in the topological analysis, the strength of noncovalent interactions decreases in the following order: O−H···O > N−H···O > C···C, O···N, C−H···O/N/(H−C).

From the above AIM and NBO discussion, we also can see that C−H···O hydrogen bonds contain critical points with very low electron density and Laplacian, and the E_{HB} and $E(2)$ energy parameters are both small so that they are very weak interaction. This means that the complexes **A6**, **B6**, **A7**, and **B7** are formed only through C−H···O interactions. Because they are unstable complexes with higher interaction energy ΔE^* than that of the remaining complexes, they are not subjected to further discussion.

The van der Waals interactions shown by the NCI tool above can also be obtained from the NBO analysis. For example, for **A1**, the interaction between H24 and C1−C6 is made to π(C1−C6) → σ^*(C22−H24) with a hyperconjugative interaction energy $E(2)$ of 1.4 kJ mol^{-}$^{-1}$ while the interaction remained between H13 and H16 is due to σ(C15−H16) → σ^*(N20−H13) transfer, 2.1 kJ mol^{-1}. The interaction between O21 and H17 of the **A4** complex is due to LP(O21) → σ^*(C15−H17), 0.4 kJ mol^{-1}, and the interaction between H24 and the benzene ring is due to $\pi_{\text{benzene ring}}$ → σ^*(C22−H24) 2.3 kJ mol^{-1}.

3.1.4. Change of O−H, N−H, and C−H Bond Lengths and Their Stretching Frequencies. To classify hydrogen bonds, we estimate a change in the length, stretching frequency, s-character in hybridization, and occupation of antibonding orbitals σ^*(X−H) (X = O, N, and C) of X−H hydrogen bonds of complexes in comparison with the original monomers, and the results are listed in Table 5. Herein, we are only interested in the intermolecular hydrogen bonds of the more stable group of complexes including **A1**, **B1**, **A2**, **B2**, **A5**, and **B5**.

For an X−H···Y hydrogen bond, according to Alabugin et al.,[51] the blue or red transition of the hydrogen bond is controlled by a balance of two main factors exerting in the opposite directions, which are the LP(Y) → σ^*(H−X) hyperconjugative interaction and the s-character increase of

https://doi.org/10.1021/acsomega.2c05023
ACS Omega 2023, 8, 11725−11735

Table 5. Changes in Lengths (Å), Stretching Frequencies (cm^{-1}), s-Character (%) in the Hybridization, and Occupation of Antibonding Orbitals σ^*(X−H) (X = O, N, and C) in X−H···Y (Y = O, N, and (H−C)) Hydrogen Bonds of Complexes in Comparison with Monomers at the MP2/aug-cc-pVDZ Level in the Gas Phase

complex	X−H···Y	Δr X−H	Δν X−H	Δ%s X−H	Δσ* X−H	complex	X−H···Y	Δr X−H	Δν X−H	Δ%s X−H	Δσ* X−H
A1	O11−H12···O21	0.0094	−186	2.96	0.0156	**B1**	O11−H12···O21	0.0089	−173	2.72	0.0144
	C6−H10···O21	−0.0013	17	0.36	0.0002		C2−H7···O21	−0.0013	13	0.38	0.0000
A2	N20−H13···O21	0.0054	−92	1.54	0.0109	**B2**	N20−H13···O21	0.0053	−90	1.53	0.0107
	C3−H8···O21	−0.0008	11	0.36	0.0001		C3−H8··O21	−0.0008	5	0.38	0.0000
							C22−H24···N20	−0.0021	22	0.70	−0.0038
A3	O11−H12···O21	0.0103	−215	3.51	0.0204	**B3**	O11−H12···O21	0.0101	−211	3.46	0.0201
A4	C22−H23···O19	−0.0023	5	0.21	−0.0021	**B4**	C22−H23···O19	−0.0025	5	0.26	−0.0023
A5	N20−H13···O21	0.0043	−69	1.72	0.0115	**B5**	N20−H13···O21	0.0041	−65	1.64	0.0113
	C15−H16···O21	−0.0009	1	0.44	0.0004						
	C3−H8···O21	−0.0014	17	0.05	0.0004		C3−H8···O21	−0.0009	7	0.50	0.0001
	C22−H24···H8−C3	−0.0018	22	0.16	−0.0025						

X in the bond. When the hyperconjugation dominates, the X−H bond elongation is reflected in a concomitant red shift of the corresponding IR stretching frequency. When the hyperconjugative interaction is weak, the s-character percentage increase leads to a shortening of the X−H bond and a blue shift in the X−H stretching frequency. As discussed above, the LP(Y) → σ^*(H−X) hyperconjugative interaction of the intermolecular hydrogen bonds O−H···O and N−H···O in **A1**, **B1**, **A2**, **B2**, **A5**, and **B5** is very large, their lengths increased in the range of 0.0041−0.0103 Å, and their stretching frequency decreased sharply about 65−215 cm^{-1}. This indicates that these hydrogen bonds belong to the red-shifted type. In general, the magnitude of an increase in the bond length and a decrease in the stretching frequency is larger for the O−H bond than for the N−H bond. Thus, the O−H···O hydrogen bond has a more downward trend of red shift than the N−H···O hydrogen bond in these complexes. The data from Table 5 show that for the C−H···O/N hydrogen bonds, the electron density in the antibonding orbital σ^*(C−H) may remain unchanged or increase or decrease slightly below 0.0038e, but all have an increased s-character, shortening the C−H bond lengths from 0.008 to 0.0025 Å and slightly increasing the stretching frequencies from 1 to 22 cm^{-1}. They are thus considered as blue-shifted hydrogen bonds.

For the hydrogen bond C22−H24···H8−C3 of **A5** when considering X is the C22 atom and Y is the (H8−C3) group, the length of the C22−H24 bond is shortened by about 0.0018 Å while its stretching frequency increased by 22 cm^{-1}. The blue-shifting of this hydrogen bond is supported by both decreasing the electron density in σ^*(C22−H24) by 0.0021e and increasing the s-character of the sp^2-hybridized orbital on the C22 atom by 0.16%.

Generally, for the more stable groups of complexes including **A1**, **B1**, **A2**, **B2**, **A5**, and **B5**, the intermolecular O−H···O and N−H···O hydrogen bonds are categorized as red-shifted while the C−H···O, C−H···N and C−H···H−C hydrogen bonds correlate with blue-shifted.

3.2. Water Solvent. The interaction energies ΔE and ΔE* of the complexes in water are listed in Figure 2 with values in italics. The most negative value of ΔE* belonging to **A3** is of −20.0 kJ mol^{-1}. Considering the more stable structures, including **A1** to **A5** and **B1** to **B5**, the absolute value of ΔE* is in the range of 16.6−20.0 kJ mol^{-1} as compared to that in the gas phase 18.3−21.7 kJ mol^{-1}. The largest interaction energy change in water is that of **A2**, with a value of only 3.7 kJ mol^{-1}. Thus, the absolute value interaction energy of the complex in water is slightly reduced as compared to that in the gas phase, meaning that the stability of the complex tends to be worse in water. This trend is consistent with the research results of Aquino et al. when studying the influence of solvents on hydrogen bonding on the interaction model of acetic acid with many different compounds; accordingly, the interaction energy in the absolute value decreases as the polarity of the solvent increases.[52]

Geometrically, the lengths of intramolecular hydrogen bonds C5−H9···O19 in water tend to increase as compared with those in the gas phase. For example, for **A1**, **A2**, **A3** and **A4**, in the gas phase they are 2.2080, 2.2095, 2.2075, and 2.2882 Å, respectively; but in water they are 2.2208, 2.2210, 2.2201, and 2.3073 Å, respectively. In contrast, intermolecular hydrogen bonds in water tend to be shorter than those in the gas phase. Intermolecular hydrogen bonds, which are stronger in the gas phase, are even shorter in solvents because these hydrogen bonds are stabilized with an increase in solvent polarity.[52] For example, for **A1**, in the gas phase, the lengths of O11−H12···O21 and C6−H10···O21 bonds are of 1.9302 and 2.7308 Å, respectively; in water, they are shortened to 1.7945 and 2.6919 Å, respectively. This observation is also available for other structures such as **B1**, **A2**, **B2**, **A3**, **B3**, **A5**, and **B5**. The shortening of intermolecular hydrogen bond lengths in solvents was also found by Mennucci in water-diazine clusters.[38] However, in the less stable complexes such as **A6**, **B6**, **A7**, and **B7**, the length of intermolecular hydrogen bonds still tends to increase (Figure 2). The lengths of the hydrogen bonds C22−H24···O19, C5−H9···O21, and C6−H10···O21 of **A6** in the gas phase are of 2.3310, 2.5258, and 2.7795 Å, respectively; they are all elongated in water with lengths of 2.3824, 2.5842, and 2.8719 Å, respectively. Notably, the A4 and B4 complexes are stabilized mainly by the C···C or O···N interactions as analyzed above, and the distance of these interactions also increases in the solvent.

4. CONCLUSIONS

The geometries, energies, and properties of the noncovalent interactions of the complex between paracetamol and formaldehyde were characterized at the MP2/aug-cc-pVDZ/aug-cc-pVTZ levels. Fourteen local minima were separately identified for the interaction between formaldehyde and two conformations of paracetamol. The interaction energies of complexes with both ZPE and BSSE corrections range from −7.0 to

https://doi.org/10.1021/acsomega.2c05023
ACS Omega 2023, 8, 11725−11735

−21.7 kJ mol^{-1}. In terms of energy, the interaction ability of paracetamol with either water or formaldehyde is the same. The strength of complexes decreases in the following order: **A1** > **B1** > **A2** > **B2** > **B3** > **A3** > **B4** > **A4** > **A5** > **B5** > **A6** > **B6** > **A7** > **B7** in the gas phase.

It is important to note that not only the hydrogen bond but also the C···C, O···N interactions heavily influence the relative stabilities of the complexes. The strength of noncovalent interactions is ordered as O−H···O > N−H···O > C···C, O···N, C−H···O/N/(H−C). For the C−H···O hydrogen bond, the intramolecular interaction is demonstrated to be more stable than the intermolecular interaction in these complexes.

It is also found that the O−H···O and N−H···O bonds in the structure of stable complexes belong to more strong red-shifted hydrogen bonds when comparing with the remaining hydrogen bonds C−H···O/N/(H−C) classified as blue-shifted.

In water, the intermolecular hydrogen bonds tend to be shortened while the intramolecular hydrogen bonds are lengthened, and the stability of the complex is slightly reduced as compared to that in the gas phase.

■ ASSOCIATED CONTENT

Supporting Information

The Supporting Information is available free of charge at https://pubs.acs.org/doi/10.1021/acsomega.2c05023.

Additional information on the quantum chemical characterizations (PDF)

■ AUTHOR INFORMATION

Corresponding Authors

Hoang Vu Dang − *Department of Analytical Chemistry and Toxicology, Hanoi University of Pharmacy, Hanoi 100000, Vietnam*; Email: hoangvd@hup.edu.vn

Hue Minh Thi Nguyen − *Faculty of Chemistry and Center for Computational Science, Hanoi National University of Education, Hanoi 100000, Vietnam*; orcid.org/0000-0001-6373-4691; Email: hue.nguyen@hnue.edu.vn

Authors

Tho Huu Nguyen − *Faculty of Natural Sciences Pedagogy, Saigon University, Ho Chi Minh City 700000, Vietnam*

Tri Huu Nguyen − *Faculty of Natural Sciences Pedagogy, Saigon University, Ho Chi Minh City 700000, Vietnam*

Thi Thanh Thuy Le − *Faculty of Natural Sciences Pedagogy, Saigon University, Ho Chi Minh City 700000, Vietnam*

Complete contact information is available at: https://pubs.acs.org/10.1021/acsomega.2c05023

Author Contributions

All authors contributed to the conceptualization and realization of the study. Tho Huu Nguyen carried out the computations and wrote the first draft. Tri Huu Nguyen and Thi Thanh Thuy Le assisted the first author in interpreting the calculated data and in preparing the manuscript. The manuscript was further edited by Hue Minh Thi Nguyen and Hoang Vu Dang. All authors have read and agreed to the published version of the manuscript.

Notes

The authors declare no competing financial interest.

■ REFERENCES

(1) Riley, K. E.; Hobza, P. Noncovalent interactions in biochemistry. *Wiley Interdiscip. Rev.: Comput. Mol. Sci.* **2011**, *1*, 3−17.

(2) Yamauchi, O. Noncovalent interactions in biocomplexes. *Phys. Sci. Rev.* **2016**, *1*, 20160001.

(3) Roblin, R. O. Confirmation of the structures of aureomycin and terramycin was one of the year's high lights in medicinal chemistry. *Chem. Eng. News* **1953**, *31*, 48−49.

(4) Yunta, M. J. R. It is important to compute intramolecular hydrogen bonding in drug design? *Am. J. Model. Optim.* **2017**, *5*, 24−57.

(5) Shankar, K.; Mehendale, H. M. Acetaminophen. In *Encyclopedia of Toxicology*, 3rd ed.; Wexler, P., Ed.; Academic Press: New York, 2014; pp 26−29.

(6) Sehrawat, R.; Tyagi, D. K.; Mittal, R.; Pandey, S. P.; Singh, O. P.; Sharma, A. K. DFT vibrational frequencies studies of acetyl-salicylic acid and Paracetamol. *Mater. Today: Proc.* **2022**, *49*, 3151−3154.

(7) Jozwiak-Bebenista, M.; Nowak, J. Z. Paracetamol: Mechanism of action, applications and safety concern. *Acta Pol. Pharm.* **2014**, *71*, 11−23. PMID: 24779190

(8) Ghasempour, H.; Dehestani, M.; Hosseini, S. M. A. Theoretical studies of the paracetamol and phenacetin adsorption on single-wall boron-nitride nanotubes: a DFT and MD investigation. *Struct. Chem.* **2020**, *31*, 1403−1417.

(9) Hoang, V. D.; Ly, D. T. H.; Tho, N. H.; Minh, T. N. H. UV spectrophotometric simultaneous determination of paracetamol and ibuprofen in combined tablets by derivative and wavelet transforms. *Sci. World J.* **2014**, *2014*, 313609.

(10) Srivastava, K.; Shimpi, M. R.; Srivastava, A.; Tandon, P.; Sinha, K.; Velaga, S. P. Vibrational analysis and chemical activity of paracetamol-oxalic acid cocrystal based on monomer and dimer calculations: DFT and AIM approach. *RSC Adv.* **2016**, *6*, 10024−10037.

(11) Misra, A. K.; Misra, M.; Panpalia, G. M.; Dorle, A. K. Interaction study of paracetamol with saturated (capric) and unsaturated (oleic) fatty acids. *Pharm. Dev. Tech.* **2007**, *12*, 423−428.

(12) Zhai, F. P.; Wei, H. E.; Liu, Y.; Hu, F. Y. Theoretical explanation for the pharmaceutical incompatibility through the cooperativity effect of the drug−drug intermolecular interactions in the phenobarbital···paracetamol···H2O complex. *J. Mol. Model.* **2019**, *25*, 181.

(13) Xu, M.; Zhang, B.; Wang, Q.; Yuan, Y.; Sun, L.; Huang, Z. Theoretical study on the hydrogen bonding interactions in paracetamol-water complexes. *J. Chil. Chem. Soc.* **2018**, *63*, 3788−3794.

(14) Dehestani, M.; Pourestarabadi, S. A density functional theory and quantum theory of atoms in molecules study on hydrogen bonding interaction between paracetamol and water molecules. *Russ. J. Phys. Chem. B* **2016**, *10*, 890−896.

(15) Danten, Y.; Tassaing, T.; Besnard, M. Density Functional Theory (DFT) calculations of the infrared absorption spectra of acetaminophen complexes formed with ethanol and acetone species. *J. Phys. Chem. A* **2006**, *110*, 8986−9001.

(16) Leyk, E.; Wesolowski, M. Interactions between paracetamol and hypromellose in the solid state. *Front. Pharmacol.* **2019**, *10*, 1−11.

(17) Srivastava, K.; Khan, E.; Shimpi, M. R.; Tandon, P.; Sinha, K.; Velaga, S. P. Molecular structure and hydrogen bond interactions of a paracetamol-4,4′-bipyridine cocrystal studied using a vibrational spectroscopic and quantum chemical approach. *CrystEngComm* **2018**, *20*, 213−222.

(18) An, G. W.; Zhang, H.; Cheng, X. L.; Zhuo, Q. L.; Lv, Y. C. Electronic structure and hydrogen bond in the crystal of paracetamol drugs. *Struct. Chem.* **2008**, *19*, 613−617.

(19) Kolesov, B. A.; Mikhailenko, M. A.; Boldyreva, E. V. Dynamics of the intermolecular hydrogen bonds in the polymorphs of paracetamol in relation to crystal packing and conformational transitions: A variable-temperature polarized Raman spectroscopy study. *Phys. Chem. Chem. Phys.* **2011**, *13*, 14243−14253.

(20) Sala, S.; Danten, Y.; Ventosa, N.; Tassaing, T.; Besnard, M.; Veciana, J. Solute−solvent interactions governing preferential

solvation phenomena of acetaminophen in CO2-expanded organic solutions: A spectroscopic and theoretical study. *J. Supercrit. Fluids* **2006**, *38*, 295−305.
(21) Sala, S.; Tassaing, T.; Ventosa, N.; Danten, Y.; Besnard, M.; Veciana, J. Molecular insight, through IR Spectroscopy, on solvating phenomena occurring in CO2-expanded solutions. *ChemPhysChem* **2004**, *5*, 243−245.
(22) Du, L.; Mackeprang, K.; Kjaergaard, H. G. Fundamental and overtone vibrational spectroscopy, enthalpy of hydrogen bond formation and equilibrium constant determination of the methanol−dimethylamine complex. *Phys. Chem. Chem. Phys.* **2013**, *15*, 10194−10206.
(23) Nassar, M. N.; Nesarikar, V. N.; Lozano, R.; Parker, W. L.; Huang, Y.; Palaniswamy, V.; Xu, W.; Khaselev, N. Influence of formaldehyde impurity in polysorbate 80 and PEG-300 on the stability of a parenteral formulation of BMS-204352: identification and control of the degradation product. *Pharm. Dev. Technol.* **2004**, *9*, 189−195.
(24) Wang, G.; Fiske, J. D.; Jennings, S. P.; Tomasella, F. P.; Palaniswamy, V. A.; Ray, K. L. Identification and control of a degradation product in Avapro film-coated tablet: low dose formulation. *Pharm. Dev. Technol.* **2008**, *13*, 393−399.
(25) Gannett, P. M.; Hailu, S.; Daft, J.; James, D.; Rybeck, B.; Tracy, T. S. In vitro reaction of formaldehyde with fenfluramine: conversion to N-methyl fenfluramine. *J. Anal. Toxicol.* **2001**, *25*, 88−92.
(26) Desai, D. S.; Rubitski, B. A.; Bergum, J. S.; Varia, S. A. Effects of different types of lactose and disintegrant on dissolution stability of hydrochlorothiazide capsule formulations. *Int. J. Pharm.* **1994**, *110*, 257−265.
(27) Pápai, I.; Jancsó, G. Hydrogen bonding in methyl-substituted pyridine−water complexes: A theoretical study. *J. Phys. Chem. A* **2000**, *104*, 2132−2137.
(28) de Carvalho, M. F.; Mosquera, R. A.; Rivelino, R. A density functional theory study of the hydrogen bond interactions in glycine dimers. *Chem. Phys. Lett.* **2007**, *445*, 117−124.
(29) Rodrigues-Oliveira, A. F.; Ribeiro, F. W. M.; Cervi, G.; Correra, T. C. Evaluation of common theoretical methods for predicting infrared multiphotonic dissociation vibrational spectra of intramolecular hydrogen-bonded ions. *ACS Omega* **2018**, *3*, 9075−9085.
(30) Chopra, N.; Kaur, D.; Chopra, G. Nature and hierarchy of hydrogen-bonding interactions in binary complexes of azoles with water and hydrogen peroxide. *ACS Omega* **2018**, *3*, 12688−12702.
(31) Boys, S. F.; Bernardi, F. The calculation of small molecular interactions by the differences of separate total energies. Some procedures with reduced errors. *Mol. Phys.* **1970**, *19*, 553−566.
(32) Frisch, M. J.; Trucks, G. W.; Schlegel, H. B.; Scuseria, G. E.; Robb, M. A.; Cheeseman, J. R.; Scalmani, G.; Barone, V.; Petersson, G. A.; Nakatsuji, H.; Li, X.; Caricato, M.; Marenich, A.; Bloino, J.; Janesko, B. G.; Gomperts, R.; Mennucci, B.; Hratchian, H. P.; Ortiz, J. V.; Izmaylov, A. F.; Sonnenberg, J. L.; Williams-Young, D.; Ding, F.; Lipparini, F.; Egidi, F.; Goings, J.; Peng, B.; Petrone, A.; Henderson, T.; Ranasinghe, D.; Zakrzewski, V. G.; Gao, J.; Rega, N.; Zheng, G.; Liang, W.; Hada, M.; Ehara, M.; Toyota, K.; Fukuda, R.; Hasegawa, J.; Ishida, M.; Nakajima, T.; Honda, Y.; Kitao, O.; Nakai, H.; Vreven, T.; Throssell, K.; Montgomery, J. A., Jr., Peralta, J. E.; Ogliaro, F.; Bearpark, M.; Heyd, J. J.; Brothers, E.; Kudin, K. N.; Staroverov, V. N.; Keith, T.; Kobayashi, R.; Normand, J.; Raghavachari, K.; Rendell, A.; Burant, J. C.; Iyengar, S. S.; Tomasi, J.; Cossi, M.; Millam, J. M.; Klene, M.; Adamo, C.; Cammi, R.; Ochterski, J. W.; Martin, R. L.; Morokuma, K.; Farkas, O.; Foresman, J. B.; Fox, D. J. *Gaussian 09 Revision C.01*; Gaussian Inc.: Wallingford CT, 2010.
(33) Lu, T.; Chen, F. Multiwfn: A multifunctional wavefunction analyzer. *J. Comput. Chem.* **2012**, *33*, 580−592.
(34) Espinosa, E.; Molins, E.; Lecomte, C. Hydrogen bond strengths revealed by topological analyses of experimentally observed electron densities. *Chem. Phys. Lett.* **1998**, *285*, 170−173.
(35) Cossi, M.; Barone, V.; Mennucci, B.; Tomasi, J. Ab initio study of ionic solutions by a polarizable continuum dielectric model. *Chem. Phys. Lett.* **1998**, *286*, 253−260.
(36) Tomasi, J.; Mennucci, B.; Cancès, E. The IEF version of the PCM solvation method: an overview of a new method addressed to study molecular solutes at the QM ab initio level. *J. Mol. Struct. THEOCHEM* **1999**, *464*, 211−226.
(37) Klamt, A.; Moya, C.; Palomar, J. A comprehensive comparison of the IEFPCM and SS(V)PE continuum solvation methods with the COSMO approach. *J. Chem. Theory and Comput.* **2015**, *11*, 4220−4225.
(38) Mennucci, B. Hydrogen bond versus polar effects: An ab initio analysis on n → π^* absorption spectra and n nuclear shieldings of diazines in solution. *J. Am. Chem. Soc.* **2002**, *124*, 1506−1515.
(39) Haisa, M.; Kashino, S.; Kawai, R.; Maeda, H. The monoclinic form of {\it p}-hydroxyacetanilide. *Acta. Crystallogr. B: Struct. Sci. Cryst. Eng. Mater.* **1976**, *32*, 1283−1285.
(40) Druzhbin, D. A.; Drebushchak, T. N.; Min'kov, V. S.; Boldyreva, E. V. Crystal structure of two paracetamol polymorphs at 20 K: A search for the 'structure-property' relationship. *J. Struct. Chem.* **2015**, *56*, 317−323.
(41) Du, J. J.; Lai, F.; Váradi, L.; Williams, P. A.; Groundwater, P. W.; Platts, J. A.; Hibbs, D. E.; Overgaard, J. Monoclinic paracetamol vs. paracetamol-4,4′-bipyridine co-crystal; what is the difference? a charge density study. *Crystals* **2018**, *8*, 46.
(42) Haisa, M.; Kashino, S.; Maeda, H. The orthorhombic form of p-hydroxyacetanilide. *Acta. Crystallogr. B: Struct. Sci. Cryst. Eng. Mater.* **1974**, *30*, 2510−2512.
(43) "Van Der Waals Radius of the elements" *Mathematica's ElementData function from Wolfram Research*, Inc. https://periodictable.com/Properties/A/VanDerWaalsRadius.an.html (accessed Oct 29, 2021).
(44) Steiner, T. The hydrogen bond in the solid state. *Angew. Chem., Int. Ed.* **2002**, *41*, 48−76.
(45) Popelier, P. *Atoms in Molecules: An Introduction*, 1st ed.; Prentice Hall, 2000.
(46) Bader, R. F. W. A quantum theory of molecular structure and its applications. *Chem. Rev.* **1991**, *91*, 893−928.
(47) Mallinson, P. R.; Woźniak, K.; Smith, G. T.; McCormack, K. L. A charge density analysis of cationic and anionic hydrogen bonds in a 'proton sponge' complex. *J. Am. Chem. Soc.* **1997**, *119*, 11502−11509.
(48) Johnson, E. R.; Keinan, S.; Mori-Sánchez, P.; Contreras-García, J.; Cohen, A. J.; Yang, W. Revealing noncovalent interactions. *J. Am. Chem. Soc.* **2010**, *132*, 6498−6506.
(49) Saleh, G.; Gatti, C.; Presti, L. L.; Contreras-García, J. Revealing non-covalent interactions in molecular crystals through their experimental electron densities. *Chemistry* **2012**, *18*, 15523−15536.
(50) Humphrey, W.; Dalke, A.; Schulten, K. VMD: Visual molecular dynamics. *J. Mol. Graph.* **1996**, *14*, 33−38.
(51) Alabugin, I. V.; Manoharan, M.; Peabody, S.; Weinhold, F. Electronic basis of improper hydrogen bonding: A subtle balance of hyperconjugation and rehybridization. *J. Am. Chem. Soc.* **2003**, *125*, 5973−5987.
(52) Aquino, A. J. A.; Tunega, D.; Haberhauer, G.; Gerzabek, M. H.; Lischka, H. Solvent effects on hydrogen bondsa theoretical study. *J. Phys. Chem. A* **2002**, *106*, 1862−1871.

https://doi.org/10.1021/acsomega.2c05023
ACS Omega 2023, 8, 11725−11735